

Cite this: *Lab Chip*, 2011, **11**, 3277

www.rsc.org/loc

PAPER

**An integrated microfluidic device for two-dimensional combinatorial dilution†**Yun-Ho Jang,<sup>‡ab</sup> Matthew J. Hancock,<sup>‡ab</sup> Sang Bok Kim,<sup>ab</sup> Šeila Selimović,<sup>ab</sup> Woo Young Sim,<sup>ab</sup> Hojae Bae<sup>ab</sup> and Ali Khademhosseini<sup>\*abc</sup>

Received 24th May 2011, Accepted 24th June 2011

DOI: 10.1039/c1lc20449a

High-throughput preparation of multi-component solutions is an integral process in biology, chemistry and materials science for screening, diagnostics and analysis. Compact microfluidic systems enable such processing with low reagent volumes and rapid testing. Here we present a microfluidic device that incorporates two gradient generators, a tree-like generator and a new microfluidic active injection system, interfaced by intermediate solution reservoirs to generate diluted combinations of input solutions within an  $8 \times 8$  or  $10 \times 10$  array of isolated test chambers. Three input solutions were fed into the device, two to the tree-like gradient generator and one to pre-fill the test chamber array. The relative concentrations of these three input solutions in the test chambers completely characterized device behaviour and were controlled by the number of injection cycles and the flow rate. Device behaviour was modelled by computational fluid dynamics simulations and an approximate analytic formula. The device may be used for two-dimensional (2D) combinatorial dilution by adding two solutions in different relative concentrations to each of its three inputs. By appropriate choice of the two-component input solutions, test chamber concentrations that span any triangle in 2D concentration space may be obtained. In particular, explicit inputs are given for a coarse screening of a large region in concentration space followed by a more refined screening of a smaller region, including alternate inputs that span the same concentration region but with different distributions. The ability to probe arbitrary subspaces of concentration space and to control the distribution of discrete test points within those subspaces makes the device of potential benefit for high-throughput cell biology studies and drug screening.

**Introduction**

Analytic, diagnostic, and screening processes in biology,<sup>1</sup> chemistry<sup>2</sup> and materials science depend heavily on techniques to prepare large arrays of samples containing multiple components at multiple concentrations. Often, these arrays of mixtures are prepared using sophisticated robotics.<sup>3</sup> Microfluidic devices offer a relatively rapid, compact and low-cost alternative and can test a range of conditions on a single sample with microlitre amounts of reagent.<sup>4</sup> Devices incorporating gradient generators or arrayed reservoirs (*e.g.* microwells)<sup>5,6</sup> are widely used<sup>7</sup> for combinatorial sample preparation; those combining both are now being developed.<sup>8–10</sup>

Microfluidic techniques for creating one-dimensional (1D) gradients of one or more components are well developed.<sup>7,11–13</sup> Common designs include the tree-like gradient generator (TLGG)<sup>14,15</sup> and other branched network devices that employ diffusion to mix contents orthogonally to the flow,<sup>11,16,17</sup> as well as convection-driven gradient devices.<sup>18,19</sup> Many of the aforementioned devices produce linear gradients, while others produce logarithmic<sup>8</sup> and exponential<sup>9</sup> gradients. Certain devices also deliver the gradient to arrays of reservoirs.<sup>10,20</sup>

Microfluidic devices for creating two-dimensional (2D) concentration gradients are relatively new,<sup>21,22</sup> and produce orthogonal gradients of multiple solutions. Existing 2D devices are partially open to the ambient air to allow for direct access to the mixed solutions. So far, on-chip sample testing and storage have not been incorporated into these devices, which would require protection from evaporation and flow-induced shear stresses.<sup>22</sup>

Microfluidic combinatorial devices for preparing mixtures of multiple component solutions in different ratios are also available.<sup>20,23–25</sup> Devices employing multiplexed channel networks are compact in size, though currently these have only generated up to 16 combinations of three to four input solutions.<sup>20,24</sup> Few microfluidic combinatorial devices incorporate gradients, which

<sup>a</sup>Center for Biomedical Engineering, Department of Medicine, Brigham and Women's Hospital, Harvard Medical School, Boston, MA, 02115, USA. E-mail: alik@rics.bwh.harvard.edu; Fax: +1 617 768 8477; Tel: +1 617 768 8395

<sup>b</sup>Harvard-MIT Division of Health Sciences and Technology, Massachusetts Institute of Technology, Cambridge, MA, 02139, USA

<sup>c</sup>Wyss Institute for Biologically Inspired Engineering, Harvard University, Boston, MA, 02115, USA

† Electronic supplementary information (ESI) available. See DOI: 10.1039/c1lc20449a

‡ Authors contributed equally.

require more complex channel networks.<sup>20,23</sup> A more powerful combinatorial device employs a valve-based mixer/multiplexer to combine up to 32 aqueous solutions in 1024 desired combinations.<sup>26</sup> The trade-off with such a device is the extended time required to prepare the mixed solutions. Here we present a device that incorporates two gradient generators, the TLGG<sup>14</sup> and a newly designed microfluidic active injection (MAI) system, interfaced by intermediate solution reservoirs to generate 100 discrete mixtures consisting of different relative concentrations of the three input solutions. Ten graded mixtures of the two TLGG input solutions were stored separately in intermediate reservoirs and then propelled into separate columns of test chambers pre-filled with a third solution. As incoming solution was injected into each test chamber (also referred to here as a deep well), flow convection and diffusion mixed the chamber contents,<sup>27</sup> increasing the concentration of the incoming solution in the chamber and reducing its concentration in fluid leaving the chamber. A discrete 1D concentration gradient was so produced by the MAI along each column of test chambers. MAI is an example of convection-driven gradient generation<sup>5,12,18,19</sup> in a cylindrical well geometry. Our versatile design can be easily modified to incorporate the MAI with other microfluidic gradient generators interfaced by the intermediate solution reservoirs. In what follows, the actions of the on-chip TLGG and MAI mechanism are first characterized independently and then in concert. The experimental results agree well with computational fluid dynamics (CFD) simulations and an approximate analytic gradient model, which taken together provide design criteria for device operation and control. Lastly, precise protocols are outlined describing how to use the device for coarse and fine screening.

## Materials and methods

### Device fabrication: 10 × 10 well design

Our device consisted of three polydimethylsiloxane (PDMS) layers: two thick layers and a thin membrane. The thick flow layer contained the TLGG which fed into ten large rectangular reservoirs ( $800 \times 400 \times 300 \mu\text{m}^3$ , 96 nL per reservoir). Each reservoir was connected by flow channels (100  $\mu\text{m}$  wide, 20  $\mu\text{m}$  high) to a series of ten cylindrical wells (300  $\mu\text{m}$  diameter, 300  $\mu\text{m}$  deep, 21.2 nL per well), defined here as a column of wells (Fig. 1). The well columns were arranged in a  $10 \times 10$  array, forming rows of wells in the perpendicular direction. The flow channels were moulded from positive photoresist and had a semi-circular cross-section to enable closure by on-chip control valves. The control valves were contained in the second 15  $\mu\text{m}$  thick PDMS membrane layer (Fig. 1D) and were controlled by channels C1–C6 in the third PDMS layer. The control valves and channels in the second and third layers comprised the MAI system. Control channel C1 was connected in series to the reservoir membranes. Control channels C2–C4 controlled valves around the wells, while C5–C6 controlled those around the reservoirs (Fig. 1A).<sup>11</sup> The device fabrication followed standard soft and photolithographic methods; additional details are outlined in the ESI (Fig. S1 and Table S1†). During device fabrication, negative pressure was applied to all control valves to avoid valve collapse and permanent bonding between PDMS layers (ESI, Fig. S1F†).

Consequently, the reservoir membranes were slightly bent upward by different amounts. This required an extra step during device operation to stretch the thin valve membranes maximally upward prior to each injection (ESI, Fig. S2B†).

### Device fabrication: 8 × 8 well design

An  $8 \times 8$  well device was fabricated to test the effect of design changes on device behaviour. The  $8 \times 8$  device had the same design as the  $10 \times 10$  device, except that the control channel C1 was connected in parallel to the reservoir membranes; the length and width of all valves were increased to  $180 \mu\text{m} \times 200 \mu\text{m}$ ; the reservoirs were circular with diameter 600  $\mu\text{m}$ ; the circular thin membranes over the reservoirs had a diameter of 500  $\mu\text{m}$ ; the reservoir and well depth was 450  $\mu\text{m}$  (127.2 nL per reservoir, 31.8 nL per well); the length of the channels between each stage of the TLGG was increased to 2.6 mm. Side channels present in the  $10 \times 10$  device for reasons unrelated to this work were removed in the  $8 \times 8$  design. The number of wells in each row and column was chosen as 8 for reasons unrelated to this work. The TLGG therefore had 2 fewer stages than the  $10 \times 10$  design. The fabrication protocol was the same as for the  $10 \times 10$  device, except that the SU-8 layer was thicker to accommodate the deeper wells and reservoirs.

### Device operation

The operation protocol for 2D gradient generation is described in Fig. 1E–I and includes two main steps: (1) generating a 1D concentration gradient of solutions A and B with the TLGG and storing the ten graded output solutions in reservoirs; and (2) using the MAI to inject the stored solutions into the array of deep wells to produce the 64 or 100 discrete mixtures with different relative concentrations of the input solutions A, B, and C (ESI, Fig. S2 and Video S1†). Initially, all flow channels and deep wells were pre-filled with solution C (Fig. 1E, blue) using a dual syringe pump (Harvard PhD 2000, Harvard Apparatus, USA). Each active injection cycle proceeded as follows. First, solutions A and B were fed from the left and right inputs, respectively, of the TLGG, simultaneously loading the 8 or 10 reservoirs (depending on design) with AB solutions of different concentrations (Fig. 1F). Stable mixtures were obtained in the reservoirs after 10, 30, and 60 min for flow rates of 60, 20, and 10  $\mu\text{L h}^{-1}$ , respectively. Negative pressure was applied to control channel C1 for approximately 1 min to stretch the membranes fully upward to force all reservoir volumes to be the same. While the reservoirs were being filled, control channel C2 sealed the main channel valves while C5 and C6 kept reservoir isolation valves open to drain excess solution into the waste channel; the excess solution did not enter the deep well array. After the reservoirs were filled, they were isolated by activating control channels C5 and C6 and halting the syringe pump (Fig. 1G). Negative pressure was applied to control channel C2 to open the corresponding reservoir valves. Positive pressure was then applied to channel C1 for 5 seconds to deflect downward the membrane valves on top of each reservoir (Fig. 1H). This pushed the stored AB solutions from each reservoir along columns of wells where the injected solutions mixed with the pre-filled solution C. Finally, control channel C2 was

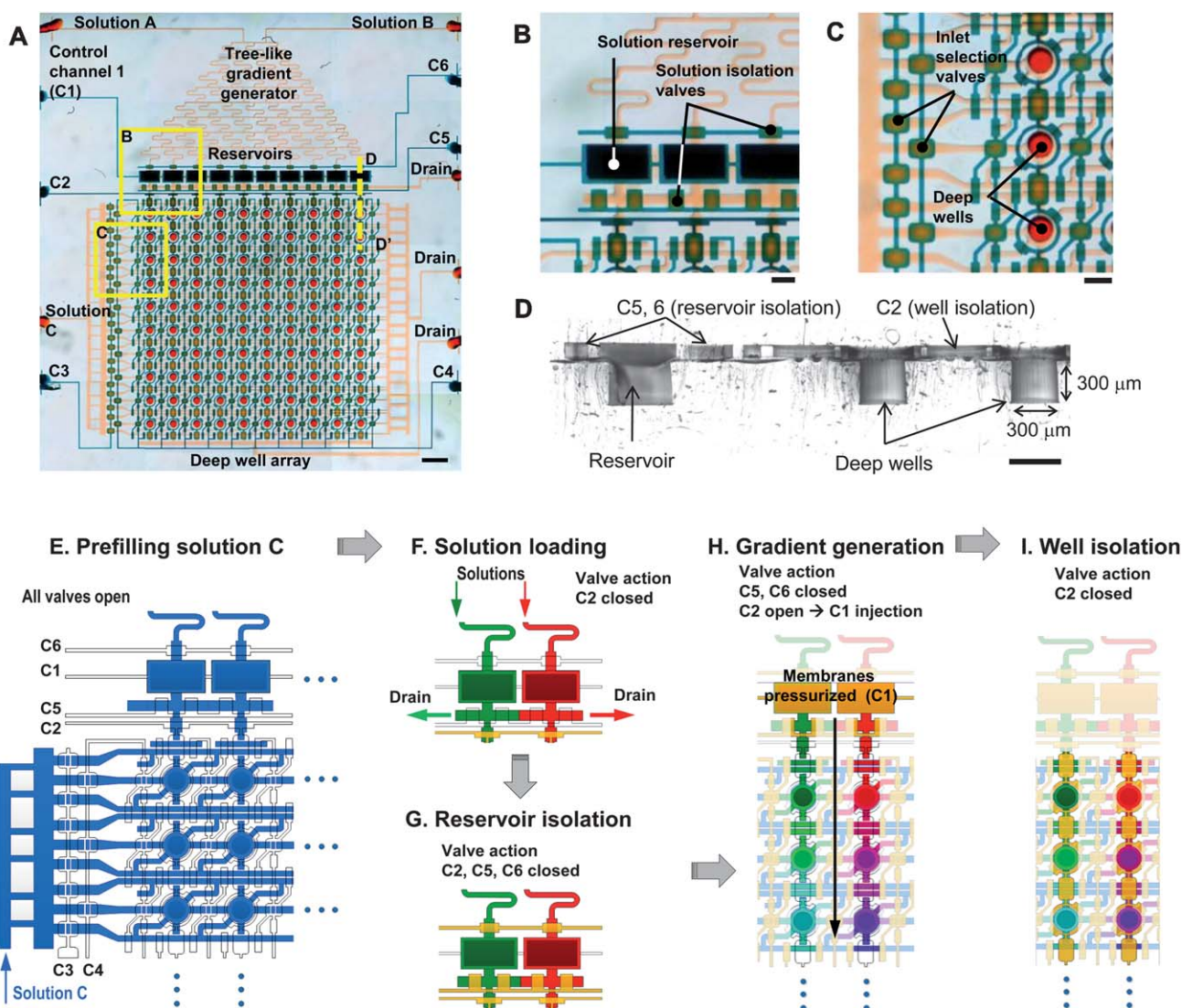


**Fig. 1** Design and operation of the 2D microfluidic combinatorial dilution device. (A) A tree-like gradient generator (TLGG) mixes two solutions inside reservoirs (black). The device also includes a  $10 \times 10$  array of deep wells (red), initially pre-filled with a third input solution, connected by flow channels (light red) and controlled by six control channels (green). The observed colour level difference is due to the disparate depths of the flow channels ( $20 \mu\text{m}$ ) and deep wells ( $300 \mu\text{m}$ ). Scale bar = 1 mm. (B) Enlarged view of reservoirs and related control valves and channels. Scale bar = 0.3 mm. (C) Enlarged view of deep wells and horizontal selection valves. Scale bar = 0.3 mm. (D) Cross-section of the device along the yellow dashed line DD' in (A) reveals reservoirs, wells, control channel C2, and a thin membrane for the microfluidic active injection (MAI) system. Scale bar = 0.3 mm. (E–G) Operational sequence to fill array of deep wells with different relative concentrations of the three input solutions. (E) The device, including wells, is pre-filled. (F) The TLGG generates graded mixtures of two solutions to be stored in the reservoirs. (G) After solutions inside reservoirs have mixed, the inlet and outlet of the reservoirs are blocked. (H) The MAI system generates discrete concentration gradients in each column of deep wells when positive pressure is applied on the C1 control channel for 5 seconds. (I) All valves are closed to isolate and maintain the mixture in each well, stabilizing the 2D combinatorial mixture across the array.

reactivated to isolate each well in the array (Fig. 1I). Additional active injection cycles filled the array to the desired degree with the AB mixtures. The time to fill the reservoirs dominated the total operation time per injection.

Valves were controlled by six control channels. Positive pressure was applied from a nitrogen tank at 100 kPa to close valves. Valves designed to be normally open were controlled *via* a solenoid valve array (Fluidigm, USA), while those normally closed were opened manually by applying negative pressure with a 3 mL plastic syringe (Becton-Dickinson).

### Characterization of MAI

We characterized the MAI system behaviour separately from the TLGG by feeding solution A at  $60 \mu\text{L h}^{-1}$  into both inputs of the TLGG, filling each reservoir with the same contents, 100% solution A, *i.e.* no gradient. The contents of each reservoir were then actively injected into the array pre-filled with solution C. In our experiment, solution A was  $100 \mu\text{M}$  fluorescein sodium salt ( $M_w$  376.27, excitation/emission wavelengths 460 nm/515 nm, Sigma-Aldrich, USA) in phosphate buffered saline (PBS, Invitrogen,

USA). The concentration in each well was quantified by the fluorescent intensity recorded by a Nikon TE2000-U microscope and analyzed with Matlab (MathWorks, USA). The well intensities were normalized by the average fluorescent intensity measured over an array pre-filled with solution A (no gradient). Three injection cycles were performed. Experiments were repeated three times for each of the three injection pressures 20, 40, and 80 kPa ( $10 \times 10$  device) and 20 and 40 kPa ( $8 \times 8$  device).

### Tracking distribution of device inputs in reservoirs and wells

The combined actions of the TLGG and MAI distributed the three device inputs across the well array. The combined effects were tracked by loading differently dyed solutions into each of the three device inputs. The device was operated as described above: solutions A and B were fed into TLGG inputs 1 and 2, respectively, and solution C was used to pre-fill the well array. Solution A was the same fluorescein salt solution used in the previous MAI experiment, solution B was 100  $\mu\text{M}$  sulforhodamine 101 ( $M_w$  606.71, excitation/emission wavelengths 586 nm/605 nm, Sigma-Aldrich, USA) dissolved in PBS, and solution C was 100  $\mu\text{M}$  calcein blue ( $M_w$  321.18, excitation/emission wavelengths 322 nm/435 nm, Sigma-Aldrich, USA) dissolved in PBS. Experiments were conducted at flow rates of 10, 20, and 60  $\mu\text{L h}^{-1}$  with an injection pressure of 40 kPa.

### Computational fluid dynamics simulations

3D computational fluid dynamics (CFD) simulations were performed to calculate the concentrations in a single column of wells over multiple injection cycles using the commercial solver CFD-ACE+ (ESI Group). The governing equations are the Navier–Stokes momentum and continuity equations and the convection-diffusion equation,<sup>28</sup>

$$\rho \left( \frac{\partial \mathbf{v}}{\partial t} + \mathbf{v} \cdot \nabla \mathbf{v} \right) = -\nabla p + \mu \nabla^2 \mathbf{v} \quad (1)$$

$$\nabla \cdot \mathbf{v} = 0 \quad (2)$$

$$\frac{\partial C}{\partial t} + \mathbf{v} \cdot \nabla C = D \nabla^2 C \quad (3)$$

respectively, where  $\mathbf{v}$  is the velocity vector,  $p$  is the pressure,  $\rho$  and  $\mu$  are the density and dynamic viscosity of the fluid, respectively,  $C$  is the concentration of solute A, and  $D$  is the molecular diffusivity. In our simulations, we used the fluid properties of water at 25 °C,  $\rho = 1000 \text{ kg m}^{-3}$  and  $\mu = 0.001 \text{ Pa s}$ , and a representative molecular diffusivity  $D = 10^{-10} \text{ m}^2 \text{ s}^{-1}$ . The computational domain (partially shown in Fig. 3A) accurately represents a single column of 10 wells in the physical device, without the main channel valves. A central difference scheme was used for spatial discretization and a first order Euler scheme was used for time discretization.

The boundary and initial conditions were as follows. A velocity of  $0.333 \text{ m s}^{-1}$  and a concentration of  $C = 1$  were imposed at the inlet of the computational domain. The inlet speed was estimated from the experimental conditions of the  $10 \times 10$  device at 80 kPa (ESI†, Methods I). The inlet concentration was assumed to be 1 due to the linearity of the convection-diffusion equation (eqn (3)). No-flux conditions were

imposed at the walls ( $\mathbf{n} \cdot \mathbf{N} = 0$ , where  $\mathbf{N} = C\mathbf{v} - D\nabla C$ ), and a convective normal flux condition was imposed at the outlet of the computational domain ( $\mathbf{n} \cdot \mathbf{N} = C\mathbf{v} \cdot \mathbf{n}$ ). The initial condition for the first injection cycle was  $C = 0$  everywhere, while the initial concentrations for subsequent cycles were the final concentrations of the previous cycle averaged across the respective well volume.

### Approximate analytic formula

We now derive an approximate analytic formula which, with one fitting parameter, reproduces the observed average well concentrations along a single column of wells following each injection cycle. Initially, the concentration in the column of wells is  $c_0$ . Solution with concentration  $c_1$  is sequentially injected into the column of wells in discrete volumes  $V_i$ . The fluid is assumed incompressible so that at each cycle a volume  $V_i$  is pumped through each well.

With simplifying assumptions we derive and solve recursive equations for the concentration in well  $m$  after cycle  $n$ . A schematic of well  $m$  is shown in Fig. S3†. We define  $c(m, n)$  as the solute concentration in well  $m$  after cycle  $n$ , and  $c_{\text{out}}(m, n)$  as that transported during cycle  $n$  through the channel between wells  $m$  and  $m + 1$ , respectively. During cycle  $n$ , a volume  $V_i$  flows into well  $m$  and a fraction  $f$  of that stays in the well, where  $0 < f < 1$  (we assume that  $f$  does not depend on  $m, n$ ). Since the fluid is incompressible, a fraction  $fV_i$  is also ejected from the well. The new solute mass in well  $m$  equals that entering from well  $m - 1$ ,  $fV_i c_{\text{out}}(m - 1, n)$  plus the existing mass not ejected,  $(V_w - fV_i)c(m, n - 1)$ , where  $V_w$  is the well volume. Dividing by  $V_w$  gives the new concentration  $c(m, n)$ ,

$$c(m, n) = fvc_{\text{out}}(m - 1, n) + (1 - fv)c(m, n - 1) \quad (4)$$

where  $v = V_i/V_w$ . The volume  $V_i$  of the fluid sent to well  $m + 1$  includes the fraction  $(1 - f)V_i$  that flowed into well  $m$ , plus  $fV_i$  ejected from well  $m$ . The solute mass transported from well  $m$  to well  $m + 1$  is thus  $(1 - f)V_i c_{\text{out}}(m - 1, n)$  plus that ejected from well  $m$ ,  $fV_i c(m, n - 1)$ . Dividing by  $V_i$  gives the solute concentration that flows from well  $m$  to well  $m + 1$ ,

$$c_{\text{out}}(m, n) = (1 - f)c_{\text{out}}(m - 1, n) + fc(m, n - 1) \quad (5)$$

The system of recursive equations (eqns (4) and (5)) determines the concentration in each well  $m$  after cycle  $n$ , subject to the conditions  $c(0, n) = c_1$  and  $c(m, 0) = c_0$  for all  $m, n \geq 1$ . The solution for all  $m, n \geq 1$  is

$$c(1, n) = c_1 + (c_0 - c_1)(1 - fv)^n \quad (6)$$

$$c(m, n) = c(1, n) + (c_0 - c_1) f^2 v n \sum_{k=2}^m (1 - fv)^{n-k+1} \times \sum_{j=0}^{k-2} \frac{(1 - fv - f)^{k-j-2} (f^2 v)^j}{j + 1} \binom{n+j}{n} \binom{k-2}{j} \quad (7)$$

where eqn (7) is valid for all  $m > 1$  and the last two bracketed terms in eqn (7) are binomial coefficients. Solutions (6) and (7) may be verified by direct substitution into eqns (4) and (5) and the initial conditions (see also the ESI†, Mathematica script).

The recursive model equations (eqns (4) and (5)) were derived based on the following simplifying assumptions. We assumed that the solutions in each well were uniformly mixed after each cycle, and the solutions were well mixed as they travelled through the channels between wells. We neglected dispersive effects and assumed that the concentration in the volume  $V_i$  remained fixed as it travelled between wells. Since the volume of the channel between wells was small relative to the well volume (*e.g.* 0.84 nL vs. 21.2 nL for the  $10 \times 10$  device), we neglected the effects of this channel in our calculations. We assumed, for example, that after each cycle the mass of solute that left one well was delivered to the next well and neglected the amount that remained in the channel between the wells.

## Results and discussion

### Characterization of the TLGG

The TLGG is a well-developed design<sup>14</sup> for generating concentration gradients of two solutions. The TLGG component of our device was designed with a variation in path lengths between the input holes and reservoirs and also incorporated a waste channel (Fig. 1). These design features produced mirror-image gradients of the two solutions input into the TLGG at low flow rates, but produced nominal differences in the gradients at larger flow rates. Our TLGG component was tested separately from other on-chip components at flow rates of 5, 10, 20, and 60  $\mu\text{L h}^{-1}$  per input stream. At 5  $\mu\text{L h}^{-1}$ , the TLGG produced nearly linear gradients; as the flow rate increased, the gradients became more nonlinear (ESI, Fig. S4†).

### Characterization of the MAI system

The MAI system was tested independent of the TLGG by feeding the same solution into both TLGG inputs (Fig. 2 and Video S1†). Two devices with similar designs, one with an  $8 \times 8$  array of wells and the other with a  $10 \times 10$  array, were tested. The graded well concentrations after successive injection cycles at an injection pressure of 20 kPa ( $8 \times 8$  design) and 80 kPa ( $10 \times 10$  design) were quantified by fluorescent intensity (Fig. 2). With each injection cycle, solution A (green) was pushed further into the array along parallel columns of wells, while being diluted and mixed with the existing pre-filled solution C (clear solution) in each deep well. Thus, the fluid leaving each well had a lower concentration of solution A than the fluid entering the well. The columns of graded well concentrations were so produced and advanced further into the array with each cycle. The standard deviations corresponding to the well concentrations plotted in Fig. 2 are given in Fig. S5†, and the corresponding column-to-column variations are plotted in Fig. S6†. The  $8 \times 8$  device had significantly lower variances in well concentrations and column-averaged concentrations than the  $10 \times 10$  device. Moreover, the injection pressure had a nominal effect on the well concentrations produced in the  $8 \times 8$  device and virtually no effect in the  $10 \times 10$  device, due to the design differences in the membranes and reservoirs (ESI, Fig. S7A†). For these pressures and a flow rate of 60  $\mu\text{L h}^{-1}$ , the second injection cycle produced a concentration profile linear up to the 8<sup>th</sup> well in the  $8 \times 8$  device and up to the 7<sup>th</sup> well in the  $10 \times 10$  device. Lastly, the variation between

the fabricated  $10 \times 10$  devices was within the run-to-run error (ESI, Fig. S7B†).

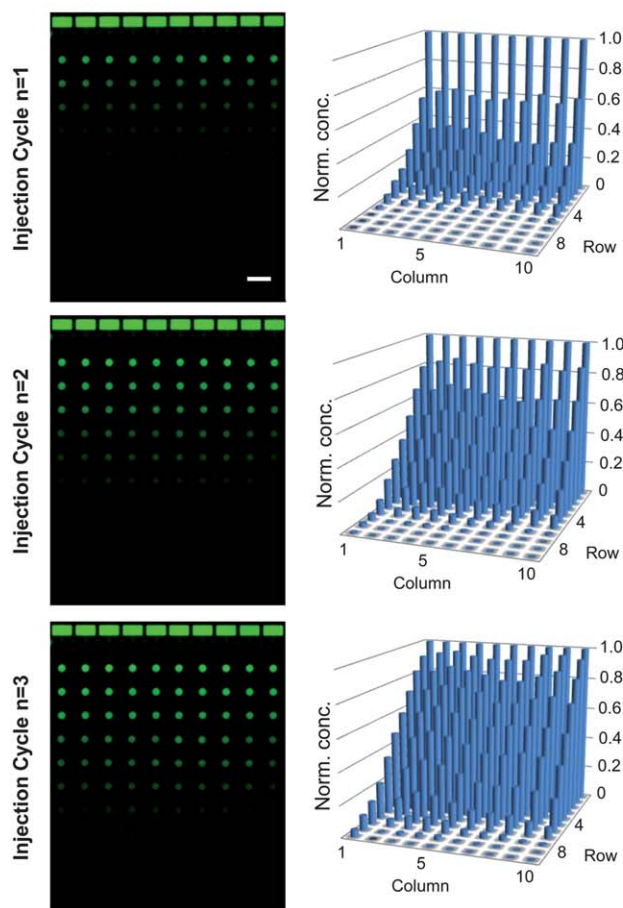
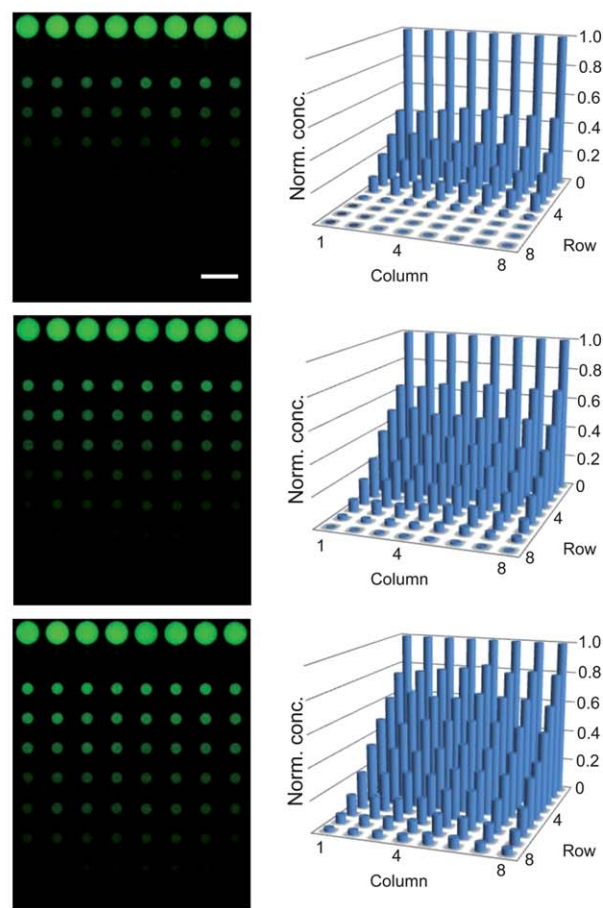
The average fluid volume injected per cycle was calculated indirectly from the total fluorescence along columns of wells. For the range of fluorescein concentrations used in our experiments, the fluorescent intensity in a well was proportional to concentration (ESI, Fig. S8A†).<sup>29</sup> Since the injected solution was fluorescent, and the pre-fill solution was not, normalizing the total intensity in a well by that in a well filled with (100%) the same fluorescent solution gave the volume fraction of injected solution in the well. Thus, summing the normalized intensities over an entire column of wells gave the volume of injected solution as a fraction of the well volume. The volume injected per cycle is the difference between the accumulated injected volumes in successive cycles, plotted in Fig. S7C† for successive injection cycles and different injection pressures. A balanced one-way analysis of variance (ANOVA) was used to test the statistical significance of the differences between the measured injected volumes at the same pressure for a given device. The level of significance was set at  $p < 0.05$ . There were no significant differences between measured injection volumes (for the same pressure and device) except for that between the first and third injections of the  $10 \times 10$  device at 80 kPa. The measured difference in injection volumes was likely due to photobleaching during operation and imaging, which occurred at approximately 3% per min under continuous UV exposure (ESI, Fig. S8B†). During device operation, the phase lamp was left on for monitoring and switched to the UV lamp for 1–3 min following each injection for imaging, approximately accounting for the measured decrease in intensity, and hence injection volume.

### CFD simulations

To rationalize the concentration dilution *via* active injection, we employed the CFD solver CFD-ACE+ to numerically solve the Navier–Stokes and convection-diffusion equations and model the flow of the injected solution along a single column of 10 wells in our device (neglecting the valves). Fig. 3A shows normalized concentrations in the first four wells after a 0.1 s flow of 0.333  $\text{m s}^{-1}$ , which modelled a single injection cycle. The concentration was virtually uniform in the channels, but decreased from well to well along each column due to dilution with the pre-filled solution (Fig. 3A and S9†). The average normalized concentration  $c$  in each well was calculated by

$$c = \frac{1}{V_w} \int_{V_w} C dV \quad (8)$$

where  $V_w$  is the well volume and  $C(x,y,z,t)$  is the normalized, instantaneous and spatially dependent concentration. The average normalized concentration  $c$  decreased along the column of wells. The simulation results agree favourably with the measured normalized well concentrations at an injection pressure of 80 kPa (Fig. 3B). Thus, our CFD simulations provide a good model for the concentration dilution by MAI. The small discrepancy is related to the apparent decrease in the injected volumes in our experiments, noted above; in our simulations, we injected a total of 40 nL each cycle.

A.  $10 \times 10$  deviceB.  $8 \times 8$  device

**Fig. 2** Characterization of the MAI system. Fluorescence images of the reservoirs and corresponding bar charts of normalized well concentrations averaged over three repetitions shown for (A) the  $10 \times 10$  and the (B)  $8 \times 8$  devices. Corresponding standard deviations are shown in Figs. S5 and S6†. Fluorescein solution (green) was fed at  $60 \mu\text{L h}^{-1}$  into both TLGG inputs, allowing the MAI system to be characterized independently. The  $10 \times 10$  device was run at 80 kPa and the  $8 \times 8$  device at 20 kPa. Scale bars = 1 mm. Norm. conc. = normalized concentration.

### Approximate analytic formula

Recursive models have been used to approximate the evolution of concentration in microfluidic gradient devices.<sup>17</sup> Based on simplifying assumptions, we derived and solved the recursive equations relevant to the graded well concentrations generated *via* MAI along a column of wells in our device (see Materials and methods). The resulting analytic formula included two coefficients: the ratio  $\nu$  of the injected volume to well volume and the fraction  $f$  of incoming fluid left in a well after one cycle. To compare with our experimental results, we set  $\nu$  to the dimensionless volume injected from each reservoir during the first injection:  $\nu = 1.5$  for the  $10 \times 10$  device at 80 kPa; and  $\nu = 1.1$  for the  $8 \times 8$  device at 20 kPa (Fig. S7C†). The parameter  $f$  could be measured from our experiments or computed from our CFD simulations. Instead, we treated  $f$  as a fitting coefficient and performed a best fit between the approximate formula (9) and the measured column-averaged normalized concentrations in the first 5 rows after 1, 2 and 3 injection cycles:  $f = 0.42$  for the  $10 \times 10$  device at 80 kPa; and  $f = 0.41$  for the  $8 \times 8$  device at 20 kPa (Fig. 3B and C). The physical interpretation of  $f = 0.42$  is that on average, approximately 42% of the incoming solution stayed in a well and pushed out the same amount of

existing well solution, while the remaining 58% bypassed the well and was mixed with the expelled well fluid in the flow channel to move downstream to other wells in the column. The approximate analytic formula with best-fit coefficient  $f$  is in relatively good agreement with the CFD simulation (Fig. 3B). Even better agreement was found between the analytic model and the  $8 \times 8$  device at 20 kPa (Fig. 3C). The nominal column-to-column variation in well concentrations due to membrane differences was noted above. To assess how these variations affected the fitting parameters in the model, we fit  $f$  separately for each column:  $f$  ranged from 0.39 to 0.45 and had a mean and standard deviation of  $0.42 \pm 0.02$ .

The predicted concentrations from both models crossed the measured values from both devices at the 5<sup>th</sup> or 6<sup>th</sup> wells (Fig. 3B and C). This discrepancy was likely due to photobleaching, since most of the fluorescent solution in the tip region originated from the first injection and was thus exposed to UV for the longest time. Further simplifying assumptions were made to derive the recursive model, though the close fit to both the experiments and simulations suggests the assumptions are valid and the analytic formula provides an adequate description of the active injection mechanism.

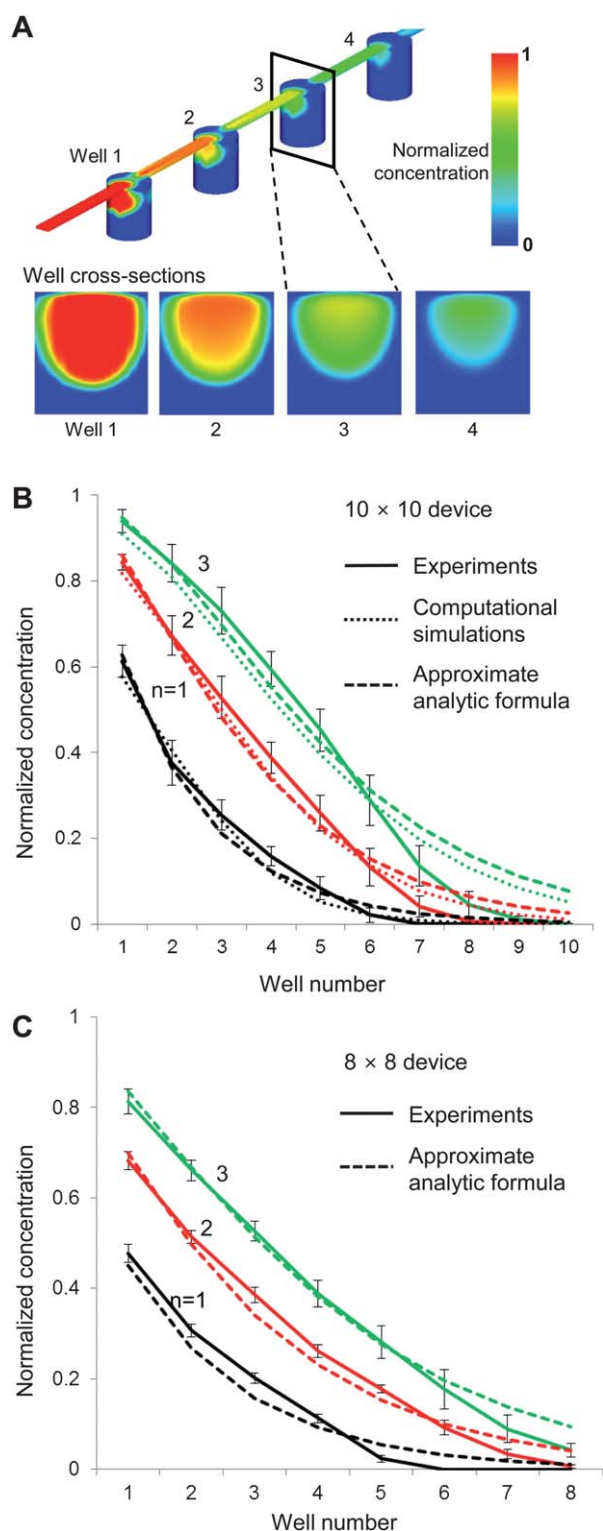


**Fig. 3** Computational simulation and analytic formula for the well concentrations generated by the MAI system. (A) 3D computational fluid dynamics (CFD) simulation of dye solution entering a column of wells connected by flow channels, closely mimicking a portion of the MAI system in our device. The 3D concentration and 2D well cross-sections illustrate the distribution of the injected fluid in successive wells. (B and C) Comparison of the normalized well concentrations along a column after one, two and three injection cycles: — column-averaged measurements; ... CFD simulations; --- analytic formula. All curves were formed

### Distribution of device inputs in reservoirs and wells

The distributions of the three device inputs in the reservoirs and wells after successive injections were fully characterized in the  $10 \times 10$  device by tagging each of the three input solutions with a different dye. The three-component well concentrations form an RGB colour palette across the deep well array for an input flow rate of  $60 \mu\text{L h}^{-1}$  (Fig. 4) and for lower flow rates (Fig. S10†). The points become more evenly distributed in concentration space with each successive injection cycle and also for lower flow rates.

To derive an empirical mathematical expression for the device behaviour, the well compositions were listed as a triplet of fractional concentrations,  $(w_{nm1}, w_{nm2}, w_{nm3})$ , where  $w_{nmk}$  is the fraction of well  $n$  that is input  $k$  after injection  $m$ . For our experiments,  $m = 0, 1, 2, 3$ ,  $k = 1, 2, 3$  and  $n = 1, 2, \dots, 100$  ( $10 \times 10$  device) and  $n = 1, 2, \dots, 64$  ( $8 \times 8$  device). Since the fluid is incompressible,  $w_{nm1} + w_{nm2} + w_{nm3} = 1$  for each  $m$  and  $n$ . Thus, when plotted in 3D concentration space ( $c$ -space), the well compositions lie in the plane  $x + y + z = 1$  (Fig. 4 and S10†).<sup>20</sup> The set of well compositions define the device output behaviour, from which all other outputs may be calculated. For example, if the three device inputs contained the concentrations  $c_1$ ,  $c_2$ , and  $c_3$  of a certain solution A, the resulting concentration of A in well  $n$  after injection  $m$  would be the weighted average

$$c_{nm} = w_{nm1}c_1 + w_{nm2}c_2 + w_{nm3}c_3 \quad (9)$$

The behaviour of our 2D combinatorial device has been fully characterized experimentally with supporting mathematical models. An empirical mathematical function has been derived from experiments to provide the output concentrations given the composition of the input solutions. We now explain the use of our device for screening applications.

### 2D combinatorial device as a screening tool

The 2D combinatorial dilution device may be used to produce 100 discrete mixtures whose compositions span any desired triangular region in the 2D space of concentrations of any two non-reacting solutions. To accomplish this, the solutions, say A and B, should be added in specific concentrations to the three inputs to our device (two TLGG ports and the pre-fill input). Here, we write the composition of the inputs as ordered pairs of concentrations for solutions X and Y, assumed to range from 0 to 1. For example, we write the first TLGG input as  $(x_1, y_1)$ , consisting of concentrations  $x_1$  and  $y_1$  of solutions X and Y, respectively. We also write the second TLGG input as  $(x_2, y_2)$  and pre-fill the well array with  $(x_3, y_3)$  (Fig. 5A). The actions of the two gradient generators (TLGG and MAI) may be visualized diagrammatically in  $c$ -space. First, the TLGG produces ten graded mixtures, stored in the reservoirs, of the two TLGG inputs. These ten mixtures are represented by a line of ten points in  $c$ -space from  $(x_1, y_1)$  to  $(x_2, y_2)$  (Fig. 5A). The pre-fill solution initially in the well array is represented by the point  $(x_3, y_3)$ .

from lines connecting the discrete well concentrations. Error bars indicate the standard deviation over three experimental runs of the same device. Results reported for the (B)  $10 \times 10$  and (C)  $8 \times 8$  designs.

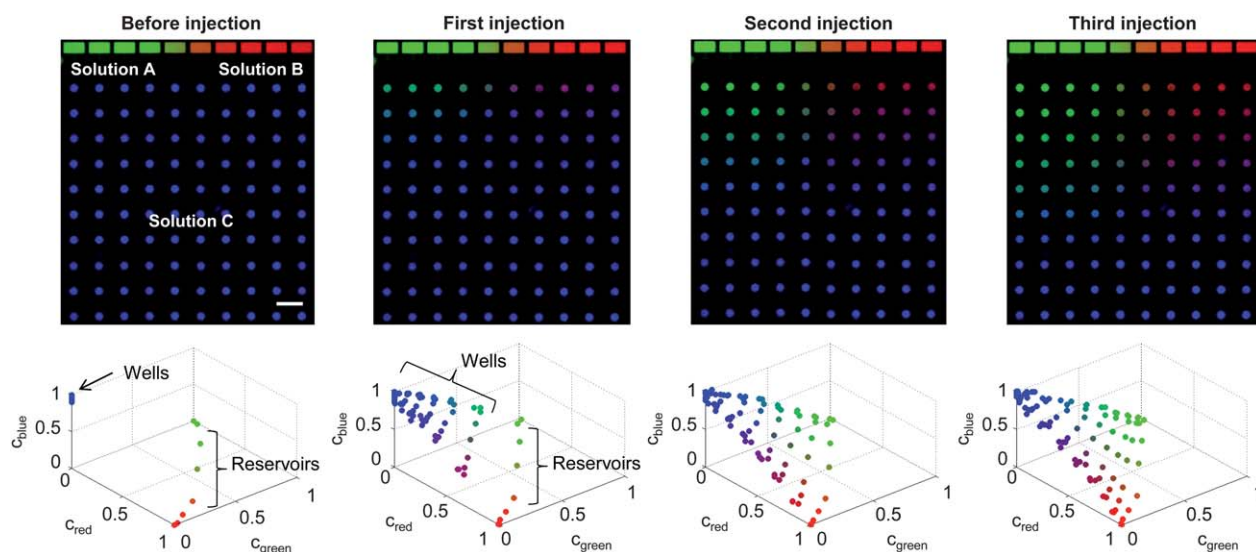


**Fig. 4** Relative distribution of the three device inputs in the reservoirs and wells. Combined action of the TLGG and MAI mechanisms filled the  $10 \times 10$  well array with different fractions of the three input solutions. The three input solutions each contained a different fluorescent dye: fluorescein sodium salt (TLGG input 1, solution A, green); sulforhodamine 101 (TLGG input 2, solution B, red); and calcein blue (pre-fill input, solution C). Before injection, all wells were pre-filled with solution C while the reservoirs contained the TLGG-generated AB mixtures. Subsequent injections propelled the AB mixtures from the reservoirs through parallel columns of wells where they were sequentially diluted. The input flow rate of the TLGG was  $60 \mu\text{L h}^{-1}$  and reservoirs were stabilized for 10 min. (Top row) Fluorescence images of the reservoirs and wells indicate their relative compositions before injection and after subsequent injection cycles. (Bottom row) Corresponding concentration space ( $c$ -space) plots of the fractional compositions of the reservoirs and wells. The points lie in the plane  $x + y + z = 1$  since the fractions add to 1. Scale bar = 1 mm.

The MAI then fills in the triangular region with discrete well concentrations between the line from  $(x_1, y_1)$  to  $(x_2, y_2)$  and the point  $(x_3, y_3)$ . As a first example, we list the precise device inputs to perform a coarse screening of two solutions  $X$  and  $Y$ . We assume all concentrations are normalized so that the full domain of possible concentrations is the square  $[0,1] \times [0,1]$  in  $c$ -space. Two runs of our 2D combinatorial dilution device are required to produce upper and lower triangles in  $c$ -space spanning the sample space  $[0,1] \times [0,1]$  (Fig. 5B). The simulated output is calculated from the empirical device output formula (9). The composition of the 100 discrete mixtures is relatively evenly distributed across each triangle in  $c$ -space (Fig. 5B), providing an effective probe of the sample space.

As a second example, we list the precise device inputs to produce 100 discrete mixtures whose compositions span an arbitrary triangular sub-region of the sample space  $[0,1] \times [0,1]$ . For the purpose of the example, we chose the triangle defined by vertices  $(0.2, 0.7)$ ,  $(0.8, 0.5)$ , and  $(0.4, 0.3)$ , which are also the ordered pairs of concentrations for the two-component input solutions. Feeding these input solutions into the device input ports, in any order, produces well concentrations spanning the same triangle in  $c$ -space (Fig. 5C). Feeding the input solutions into different input ports alters the well concentration distribution, but spans the same  $c$ -space triangle (Fig. 5C). Thus, our device not only allows arbitrary probing of 2D  $c$ -space, but also allows a certain level of control over both the composition of the solution input to a given input port and the distribution of well concentrations within each sub-region of 2D  $c$ -space. We validated the coarse and fine protocols by inputting sulforhodamine (red) and fluorescein (green) dyes in specific concentrations into the three input ports of our  $10 \times 10$  device (Fig. 5D). The dimensionless concentrations listed in Fig. 5D were obtained

by dividing the physical concentrations by  $100 \mu\text{M}$ , the maximum dye concentration. Given the above protocols, possible immediate applications are drug<sup>30</sup> or growth factor screening.<sup>31</sup>

#### Additional remarks

Our device has several advantages over existing approaches. (1) The MAI mechanism can generate a graded sequence of well concentrations in seconds with one injection cycle. The underlying convection-based mixing is orders of magnitude faster than diffusion-limited mixing.<sup>11,18,19</sup> The MAI reduces the overall preparation time of the 2D gradient, important for time-sensitive applications such as cytotoxicity studies. (2) The MAI mechanism may be readily combined with gradient generators, such as the TLGG in the present work, to create 2D combinatorial mixtures. In fact, replacing the TLGG in our device with a second MAI system could dramatically reduce the overall device operation time. (3) The sequence of well concentrations can be tuned by adjusting the flow rate and the number of injection cycles. (4) The MAI mechanism is integrated with the deep well array, making the device compact and allowing the combinatorial mixtures to be isolated in the deep wells. As in a similar device, cells would be loaded with the pre-fill solution and allowed to settle to the base of the wells, where they would be protected from the flow shear induced by active injection.<sup>32</sup> (5) Finally, the MAI mechanism dispenses into and traps in each well a finite liquid volume, enabling discrete increments of soluble factors to be tested on a sample.

Further improvements could be made to our 2D combinatorial dilution device. (1) The column-to-column and device-to-device variation could be improved by increasing the design and

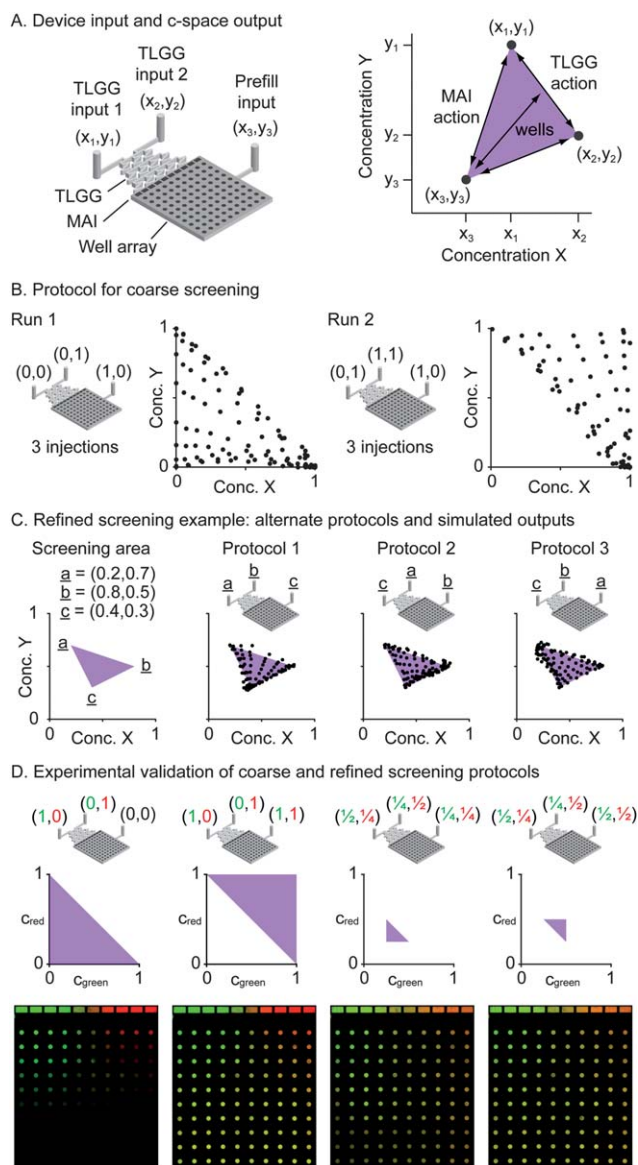


**Fig. 5** The 2D combinatorial dilution device as a screening tool. (A) Diagram of the device indicating inputs to TLGG and well pre-fill. Inputs given as ordered pairs of concentrations for solutions  $X$ ,  $(x_1, x_2, x_3)$  and  $Y$ ,  $(y_1, y_2, y_3)$ , assumed to range from 0 to 1. Schematic of the region in  $c$ -space spanned by well and reservoir concentrations. The combined effects of the component gradient generators (TLGG, MAI) are illustrated. (B) Protocol for coarse screening requires two runs of the device to produce upper and lower triangles in  $c$ -space spanning the entire range of diluted combinations. Conc. = concentration. (C) The refined screening of a triangular sub-region of  $c$ -space (purple). The three protocols each span the screening triangle, but produce different distributions in  $c$ -space. All output well and reservoir concentrations were calculated from the output formula (9) derived from experimental data. (D) Experimental validation of the coarse and refined screening protocols. The device inputs are illustrated at the top, the triangular screening regions are shown below, followed by the resulting fluorescence images.

fabrication uniformity of the thin membranes inside the MAI injectors. The assembly of the device currently requires careful alignment; improved designs could simplify assembly. (2) Due to the relatively small well volumes (20 nL), maintaining constant conditions in a well for prolonged durations could require

additional injection cycles to replace liquid absorbed by the PDMS or, in the case of cell-based applications, soluble factors consumed by cells. However, in isolated wells of similar volumes ( $\sim 20$  nL), 50–100 cells per well remained at least 88% viable when incubated for at least 24 h without media replacement.<sup>6,32</sup> For longer durations, a multi-step experimental protocol involving a solution replacement step and a gradient re-generation step could overcome this issue. (3) The MAI establishes a concentration profile *via* rapid injection ( $>0.3$  m s<sup>-1</sup>) of solution from channels to deep wells. The complex fluidic behaviour may hinder design modifications for obtaining arbitrary profiles from the MAI mechanism. Despite the flow complexity, we derived simple mathematical expressions that adequately described the resulting average concentrations; similar approaches could be used for modified designs. (4) Creating particle gradients with the injection mechanism would be problematic due to clogging, while gradients of larger molecules such as polymer solutions would require more time for diffusion to mix solutions in each well between injection cycles. Other mechanisms exist for these purposes.<sup>5,18</sup> (5) Finally, since the active injection mechanism uses the wells as dilution mechanisms, the contents of the wells during pre-fill and intermediate injections generally differ from the final combinatorial mixtures. Thus, for applications involving cells, which would generally be loaded with or before the pre-fill solution, the cells would be exposed to intermediate well mixtures during device operation. Related side-effects could be reduced by expediting the formation of the combinatorial well contents. Moreover, feeding three input solutions into the input ports in any order yields well concentrations spanning the same triangle in  $c$ -space (Fig. 5C). Thus, for a particular screening, the user is given some flexibility as to the input composition and could, for example, load the least reactive or harmful components/concentrations into the pre-fill solution.

## Conclusions

In this paper we presented a new integrated microfluidic device incorporating two gradient generators, the TLGG and MAI, that, in concert, produced graded combinations of three input solutions across  $8 \times 8$  or  $10 \times 10$  arrays of deep wells. The compositions of the solutions stored in the arrays were evenly distributed across planar concentration surfaces, rendering the device ideal for combinatorial and dosimetry studies. In particular, precise protocols were given to use the device as a screening platform to investigate the synergistic effects of pairs of factors on biological entities. The functionality of the active injection mechanism was adequately modelled by both computational simulations and an approximate analytic formula, providing ample design criteria for future device use and modification. The device design is naturally scalable to larger arrays, while other combinatorial concentrations may be obtained by using other existing gradient generators.

## Author contribution

YHJ, MJH, WYS, ŠS, HB and AK designed the study. YHJ and WYS designed and fabricated the device. YHJ performed the gradient experiments. YHJ, MJH, and ŠS analyzed the data. MJH developed the analytic model. SBK performed the

computer simulations. YHJ, MJH, ŠS, SBK, and WYS wrote the paper. AK supervised the research. All authors discussed the results, commented on the manuscript, and agreed on its contents.

## Acknowledgements

This paper was supported by the National Institutes of Health (EB008392; HL092836; DE019024; EB012597; DE021468), the National Science Foundation (DMR0847287), the Institute for Soldier Nanotechnology, the Office of Naval Research, and the US Army Corps of Engineers. Y. H. Jang was partially supported by the National Research Foundation of Korea (Grant NRF-2009-352-D00107).

## References

- 1 B. F. Rasmussen, A. M. Stock, D. Ringe and G. A. Petsko, *Nature*, 1992, **357**, 423–424.
- 2 P. H. Masscheleyn, R. D. Delaune and W. H. Patrick, *Environ. Sci. Technol.*, 1991, **25**, 1414–1419.
- 3 C. J. Flaim, S. Chien and S. N. Bhatia, *Nat. Methods*, 2005, **2**, 119–125; H. Tavana, A. Jovic, B. Mosadegh, Q. Y. Lee, X. Liu, K. E. Luker, G. D. Luker, S. J. Weiss and S. Takayama, *Nat. Mater.*, 2009, **8**, 736–741; D. G. Anderson, S. Levenberg and R. Langer, *Nat. Biotechnol.*, 2004, **22**, 863–866.
- 4 A. Khademhosseini, R. Langer, J. Borenstein and J. Vacanti, *Proc. Natl. Acad. Sci. U. S. A.*, 2006, **103**, 2480–2487.
- 5 J. He, Y. Du, J. L. Villa-Urbe, C. Hwang, D. Li and A. Khademhosseini, *Adv. Funct. Mater.*, 2010, **20**, 131–137.
- 6 J. Wu, I. Wheeldon, Y. Guo, T. Lu, Y. Du, B. Wang, J. He, Y. Hu and A. Khademhosseini, *Biomaterials*, 2011, **32**, 841–848.
- 7 T. M. Keenan and A. Folch, *Lab Chip*, 2008, **8**, 34–57.
- 8 L. Kim, M. D. Vahey, H. Y. Lee and J. Voldman, *Lab Chip*, 2006, **6**, 394–406.
- 9 A. Cappiello, G. Famigliani, C. Fiorucci, F. Mangani, P. Palma and A. Siviero, *Anal. Chem.*, 2003, **75**, 1173–1179.
- 10 P. J. Hung, P. J. Lee, P. Sabounchi, N. Aghdam, R. Lin and L. P. Lee, *Lab Chip*, 2005, **5**, 44–48; P. J. Hung, P. J. Lee, P. Sabounchi, R. Lin and L. P. Lee, *Biotechnol. Bioeng.*, 2005, **89**, 1–8; Š. Selimović, W. Y. Sim, S. B. Kim, Y.-H. Jang, W. G. Lee, M. Khabiry, H. Bae, S. Jambovane, J. W. Hong and A. Khademhosseini, *Anal. Chem.*, 2011, **83**, 2020–2028.
- 11 B. Mosadegh, M. Agarwal, H. Tavana, T. Bersano-Begey, Y.-s. Torisawa, M. Morell, M. J. Wyatt, K. S. O'Shea, K. F. Barald and S. Takayama, *Lab Chip*, 2010, **10**, 2959–2964.
- 12 M. J. Hancock, J. He, J. F. Mano and A. Khademhosseini, *Small*, 2011, **7**, 892–901.
- 13 K. Sun, Z. Wang and X. Jiang, *Lab Chip*, 2008, **8**, 1536–1543.
- 14 N. L. Jeon, S. K. W. Dertinger, D. T. Chiu, I. S. Choi, A. D. Stroock and G. M. Whitesides, *Langmuir*, 2000, **16**, 8311–8316.
- 15 S. K. W. Dertinger, D. T. Chiu, N. L. Jeon and G. M. Whitesides, *Anal. Chem.*, 2001, **73**, 1240–1246; N. L. Jeon, H. Baskaran, S. K. W. Dertinger, G. M. Whitesides, L. Van De Water and M. Toner, *Nat. Biotechnol.*, 2002, **20**, 826–830; E. Cimetta, C. Cannizzaro, R. James, T. Biechele, R. Moon, N. Elvassore and G. Vunjak-Novakovic, *Lab Chip*, 2010, **10**, 3277–3283.
- 16 K. Lee, C. Kim, B. Ahn, R. Panchapakesan, A. R. Full, L. Nordee, J. Y. Kang and K. W. Oh, *Lab Chip*, 2009, **9**, 709–717; K. Hattori, S. Sugiura and T. Kanamori, *Lab Chip*, 2009, **9**, 1763–1772; S. Sugiura, K. Hattori and T. Kanamori, *Anal. Chem.*, 2010, **82**, 8278–8282; W. Saadi, S. W. Rhee, F. Lin, B. Vahidi, B. G. Chung and N. L. Jeon, *Biomed. Microdevices*, 2007, **9**, 627–635.
- 17 D. Irimia, D. A. Geba and M. Toner, *Anal. Chem.*, 2006, **78**, 3472–3477.
- 18 Y. Du, M. J. Hancock, J. He, J. L. Villa-Urbe, B. Wang, D. M. Cropek and A. Khademhosseini, *Biomaterials*, 2010, **31**, 2686–2694.
- 19 Y. Du, J. Shim, M. Vidula, M. J. Hancock, E. Lo, B. G. Chung, J. T. Borenstein, M. Khabiry, D. M. Cropek and A. Khademhosseini, *Lab Chip*, 2009, **9**, 761–767.
- 20 K. Lee, C. Kim, Y. Kim, B. Ahn, J. Bang, J. Kim, R. Panchapakesan, Y.-K. Yoon, J. Kang and K. Oh, *Microfluid. Nanofluid.*, 2011, **11**, 75–86.
- 21 J. Atencia, J. Morrow and L. E. Locascio, *Lab Chip*, 2009, **9**, 2707–2714; B. G. Chung, F. Lin and N. L. Jeon, *Lab Chip*, 2006, **6**, 764–768.
- 22 G. A. Cooksey, C. G. Sip and A. Folch, *Lab Chip*, 2009, **9**, 417–426.
- 23 C. Neils, Z. Tyree, B. Finlayson and A. Folch, *Lab Chip*, 2004, **4**, 342–350.
- 24 K. Lee, C. Kim, G. Jung, T. S. Kim, J. Y. Kang and K. W. Oh, *Microfluid. Nanofluid.*, 2010, **8**, 677–685; D. Titmarsh and J. Cooper-White, *Biotechnol. Bioeng.*, 2009, **104**, 1240–1244.
- 25 M. C. Liu, D. Ho and Y. C. Tai, *Sens. Actuators, B*, 2008, **129**, 826–833.
- 26 C. L. Hansen, M. O. A. Sommer and S. R. Quake, *Proc. Natl. Acad. Sci. U. S. A.*, 2004, **101**, 14431–14436.
- 27 P. N. Shankar, *J. Fluid Mech.*, 1997, **342**, 97–118; P. N. Shankar and M. D. Deshpande, *Annu. Rev. Fluid Mech.*, 2000, **32**, 93–136.
- 28 M. A. Holden, S. Kumar, E. T. Castellana, A. Beskok and P. S. Cremer, *Sens. Actuators, B*, 2003, **92**, 199–207.
- 29 F. Lin, W. Saadi, S. W. Rhee, S. J. Wang, S. Mittal and N. L. Jeon, *Lab Chip*, 2004, **4**, 164–167.
- 30 N. Ye, J. Qin, W. Shi, X. Liu and B. Lin, *Lab Chip*, 2007, **7**, 1696–1704.
- 31 L. H. Lee, R. Peerani, M. Ungrin, C. Joshi, E. Kumacheva and P. Zandstra, *Stem Cell Res.*, 2009, **2**, 155–162.
- 32 Y.-H. Jang, C. H. Kwon, S. B. Kim, Š. Selimović, W. Y. Sim, H. Bae and A. Khademhosseini, *Biotechnol. J.*, 2011, **6**, 156–164.